Quantum-Dot-Induced Self-Assembly of Cricoid Protein for Light Harvesting

Lu Miao, Jishu Han, Hao Zhang, Linlu Zhao, Chengye Si, Xiyu Zhang, Chunxi Hou, Quan Luo, Jiayun Xu, and Junqiu Liu*

State Key Laboratory of Supramolecular Structure and Materials, College of Chemistry, Jilin University, 2699 Qianjin Street, Changchun 130012, China

ABSTRACT Stable protein one (SP1) has been demonstrated as an appealing building block to design highly ordered architectures, despite the hybrid assembly with other nano-objects still being a challenge. Herein, we developed a strategy to construct high-ordered protein nanostructures by electrostatic self-assembly of cricoid protein nanorings and globular quantum dots (QDs). Using multielectrostatic interactions between 12mer protein nanoring SP1 and oppositely charged CdTe QDs, highly ordered nanowires with sandwich structure were achieved by hybridized self-assembly. QDs with different sizes (QD1, 3−4 nm; QD2, 5−6 nm; QD3, ∼10 nm) would induce the self-assembly protein rings into various nanowires, subsequent bundles, and irregular networks in aqueous solution. Atomic force microscopy, transmission electron microscopy, and dynamic light scattering characterizations confirmed that the size of QDs and the structural topology of the nanoring play critical functions in the formation of the superstructures. Furthermore, an ordered arrangement of QDs provides an ideal scaffold for designing the light-harvesting antenna. Most importantly, when different sized QDs (*e.g.*, QD1 and QD3) self-assembled with SP1, an extremely efficient Förster resonance energy transfer was observed on these protein nanowires. The self-assembled protein nanostructures were demonstrated as a promising scaffold for the development of an artificial light-harvesting system.

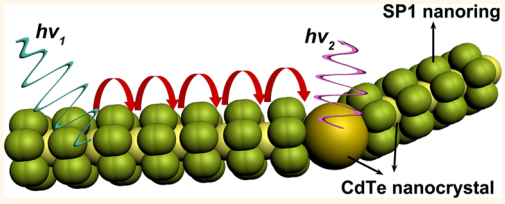

KEYWORDS: protein self-assembly · quantum dot · nanowire · light harvesting · SP1 · electrostatic interaction

The development of supramolecular nanostructures on the basis of assembled functional biomolecules has attracted great interests due to their biocompatibility, biodegradability, and defined morphology.[1−5] In particular, proteins as indispensable biomacromolecules have successfully been used to fabricate self-assembled nanostructures because of their well-defined morphology, recognition capability, and specific reactivity toward target molecules, where the nanostructures hold great potential for practical applications such as tissue engineering, biomineralization, light harvesting, and drug delivery systems.[6−9] However, the design of protein self-assembly architectures is highly challenging owing to the chemical and structural heterogeneity of protein surfaces. Understanding the structural information of protein surfaces and choosing the appropriate driving forces for self-assembly will promote the engineering of protein-based supramolecular nanostructures.

In recent years, various strategies have been devoted to construct high-ordered protein nanostructures. For example, a nanotube comprising ring-like protein Hcp1 was constructed by steric and chemical complementarity and stabilized by engineered disulfide bonding.[10] A 2D network was constructed by an interprotein heme−heme pocket interaction between modified cytochrome b_{562} protein and its synthetic heme analogue.[11] Furthermore, Yeates and co-workers have recently developed a series of large symmetrical molecular cages, filaments, layers, and porous materials with a fusion protein, engineered using one molecule each of protein A and B, which naturally forms self-assembling oligomers.[12] Over the years, our group has made continued efforts to construct high-ordered nanostructures. For instance, protein nanowires and nanorings were successfully prepared by protein self-assembly through host−guest interaction and metal coordination.[13−15] However, the development of novel assembly strategy to construct functional protein nanostructures remains a significant challenge.

Electrostatic self-assembly of biomacromolecules, especially protein-based self-assembly, has emerged as a powerful approach for the construction of various

* Address correspondence to junqiuliu@jlu.edu.cn.

Received for review January 21, 2014 and accepted March 6, 2014.

Published online March 06, 2014
10.1021/nn500414u

© 2014 American Chemical Society

hierarchical nanostructures over the past decade.[16,17] Not only are their high-ordered assemblies important for molecular recognition, drug delivery, and sensing applications, but they are also interesting from a scientific point of view to understand and subsequently develop new self-assembled structures and materials.[18−22] Kostiainen *et al.* reported a hierarchical electrostatic assembly process, using protein cages with various polymers or core−shell nanoparticles (NPs).[23−25] On the basis of molecular dynamic simulations, they modulated the properties of the final assembly by modifying the dendritic generation or other critical parameters which control the molecular recognition between dendritic constructs and viruses.[18] Furthermore, the highly ordered superstructures exhibited the ability to tune magnetic properties of NPs.[26] Nevertheless, there is no report on the construction of high-ordered protein nanowires by electrostatic interaction-driven self-assembly so far.

We therefore sought to utilize an electrostatic self-assembly method to prepare high-ordered nanostructures with a special protein, stable protein one (SP1). It is a ring-like protein consisting of 12 subunits that are tightly bound to each other *via* hydrophobic interactions forming a double-layered six-membered ring.[27] According to the analysis of the crystal structure of SP1 protein, it can be employed as an appealing building block for electrostatic self-assembly due to its higher symmetric and negatively charged hydrophilic structure at neutral pH. In particular, most of the acidic amino acids are distributed on the top and bottom surface of the dodecamer SP1. In addition, SP1 has extremely high thermal and chemical stability. For example, its melting temperature is 107 °C, and it exhibits a pronounced resistance to detergents, such as sodium dodecyl sulfate (SDS), and proteases.[27] Taking advantage of its unique structure and distinctive chemical characteristics, several research groups make use of natural or modified SP1 nanorings for nanobiotechnology and biomaterials applications.[28−30] For example, Shoseyov and co-workers constructed high-ordered nanowires assembled with the SP1 nanoring that interacted with gold nanoparticles through metal coordination interaction.[29]

Here we present semiconductor quantum dots (QDs) as linkers to induce SP1 nanorings into significantly ordered self-assembled structures. Several favorable characteristics of QDs including tunable optical properties, photostability, relatively high quantum yield (QY), and the ability for doping with other elements make them increasingly interesting in various applications.[31−34] Integration of unique optical or electronic properties of QDs along with the ability to assemble these semiconductor materials with engineered biological scaffolds or templates can yield novel nanoscale systems. In particular, their capability to harvest visible light energy can address limitations of current approaches to manufacturing light-driven devices.[35−40]

In this paper, we developed a novel strategy for constructing high-ordered protein nanostructures by electrostatic self-assembly of cricoid protein nanorings and globular QDs. The QDs with different sizes induce the protein rings into various highly ordered nanostructures in aqueous solution. Meanwhile, the significantly ordered arrangement of the QDs makes the self-assembled protein nanowires an ideal scaffold for designing an efficient light-harvesting system.

RESULTS AND DISCUSSION

The SP1 protein was prepared using a typical genetic expression method, and the purification of protein was verified using sodium dodecyl sulfate polyacrylamide gel electrophoresis (SDS-PAGE) and TEM analysis (Supporting Information Figure S1). Ring-like SP1, with a diameter of approximately 11 nm, a central hole of 2−3 nm, and a width of 4−5 nm, was well-distributed in aqueous solution. The charge distribution on the SP1 protein surface is shown in Figure 1a. Acidic amino acids (negative charges, red color) are distributed all around the protein, especially the top and bottom surface of the dodecamer SP1. For the three kinds of CdTe QDs prepared from mercaptoethylamine (MA), positive charges covered the QDs (Figure 1b). The diameter of these CdTe QDs are 3−4 nm (QD1), 5−6 nm (QD2), and ∼10 nm (QD3). Owing to the electrostatic interaction and spatial complement, the positively charged QDs are capable of being sandwiched between two SP1 nanorings and give full control of the protein orientation on the surface of the QDs, which consequently induces the self-assembly of proteins into highly ordered 1D nanowires (Figure 1c).

Figure 2 shows tapping mode atomic force microscopy (AFM) images of SP1-QD assembly. Numerous high-ordered SP1 protein nanowires, with several hundred nanometers in length, are observed, driven by QD1 and QD2 (Figure 2a,d). Such structures are spontaneously formed upon incubation of SP1 and QDs in aqueous solution. Figure 2g shows the protein nanoarrays that result from the binding of SP1 with QD3. It displays complex nanoarchitectures including the curved nanolines or a fork in the curved line as shown in the scheme of Figure 2g. The structural differences demonstrate that the size of the QDs is the key for inducing SP1 protein into various nanostructures. When the size of the QDs is small (*e.g.*, QD1 and QD2), QDs fit well for the central hole of the SP1 nanoring, and straight nanowires are formed according to the spatial complement, but while the size is large (*e.g.*, QD3), multiple SP1 nanorings connected to one QD and various nanostructures are constructed.

The uniform height (∼9 nm) of the nanostructures shown in Figure 2b,e is slightly lower than the diameter

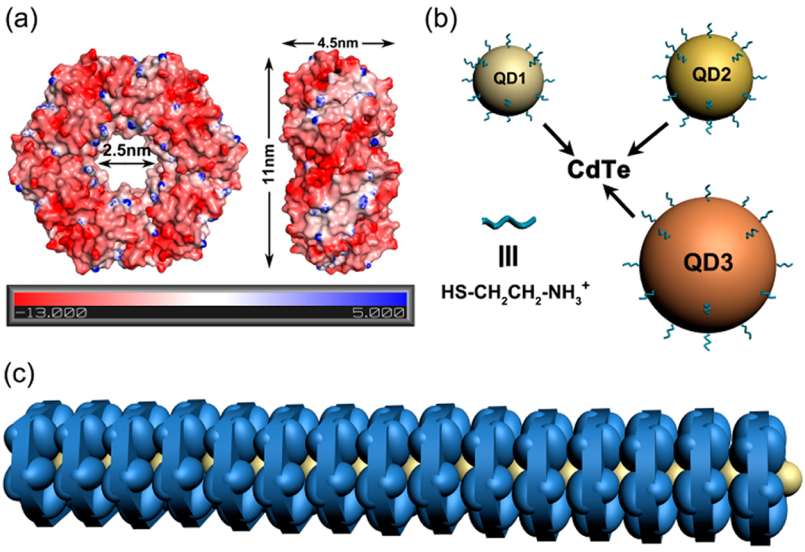

Figure 1. Design of the self-assembled SP1-QD nanowires. (a) Top view and side view of the SP1 nanoring structure with charge distribution on the surface. The red color is for negative charges, and blue color is for positive charges. (b) Three kinds of CdTe QDs were capped with mercaptoethylamine (positive charges) where the diameters of QDs are 3−4 nm (QD1), 5−6 nm (QD2), and ~10 nm (QD3). (c) Model of a SP1 nanowire formed by the self-assembly of SP1 nanoring subunits (blue) and QDs (yellow balls).

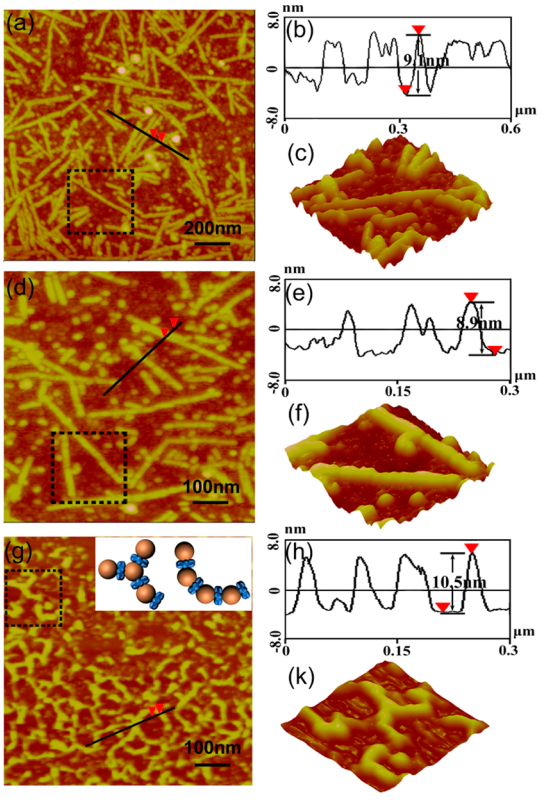

Figure 2. AFM images of the self-assembled nanostructures by cricoid SP1 nanoring and different sized CdTe QDs. (a,d, g) AFM topographical images of the nanostructures assembled by SP1 with QD1, QD2, and QD3, respectively; (b, e,h) associated height profile along the black line in panels (a), (d), and (g); (c,f,k) 3D images of the squares in (a), (d), and (g). The inset in (g) shows the scheme representing the formation assembled by SP1 and QD3.

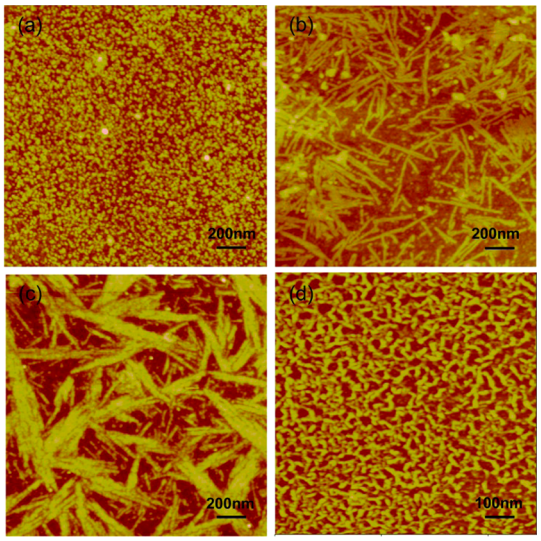

Figure 3. AFM images of SP1-QD assembly at high concentration. (a) Wild-type SP1. (b) SP1-QD1 assembly. (c) SP1-QD2 assembly. (d) SP1-QD3 assembly. The final concentration of SP1 is 125 mg/L, and the final concentrations of QDs are 2.5, 6.25, and 25 μM, respectively.

of the crystal structure of the single SP1 nanoring (11 nm). The slight decrease is probably due to the resistance of side profile of the "standing" SP1 ring to the tip force and/or loss of hydration from the protein since AFM imaging was carried out in air.[29] The height profile of Figure 2h is quite reasonable for the expected QD3 structure. Figure 2c,f,k displays 3D images of the square in Figure 2a,d,g, demonstrating the homogeneity of the nanostructures. Interestingly, when we increased the concentrations of SP1 and QDs, obvious differences in assemblies with different sizes of QDs were clearly observed (Figure 3). There are a large number of nanowires uniformly distributed in the AFM image of the SP1-QD1 system (Figure 3b); bundles

of nanowires are observed in the SP1-QD2 assembly (Figure 3c); moreover, a planar network driven by SP1 and QD3 was produced when the protein concentration was increased to 125 mg/L (Figure 3d).

Transmission electron microscope (TEM) images of the self-assembly architectures (Figure 4) support the AFM findings. Figure 4a,b displays the TEM images (negatively stained with sodium phosphotungstate) of the nanowires assembled using the SP1 nanoring with QD1 and QD2, respectively. Several separated SP1 nanorings marked by dotted squares are clearly observed. From the measurement of diameters of the dots sitting on the center of the SP1 nanoring (3.3 and 5.6 nm, consistent with the size of QD1 and QD2), we confirm the attachment of QDs to the center of the SP1 protein. As expected, the suitable sizes of QD1 and QD2 make them fit well into the SP1 inner pore. In addition, once attached to the SP1 nanoring, the QDs can further serve as the linker to create SP1-QD chains as shown in the AFM and TEM images.

If observed carefully, tightly arranged SP1-QD1 chains are found (Figure 4a). In contrast, the spacings of adjacent SP1 nanorings in SP1-QD2 assembly are slightly larger such that QD2 appears clearly as dark spots in Figure 4b (the dots marked by black arrows). Furthermore, when we increased the concentrations of ingredients 5-fold, even longer nanowires but no more than two parallel lines of the SP1-QD1 system are observed (Figure S2a). Figure 4c and Figure S2b show

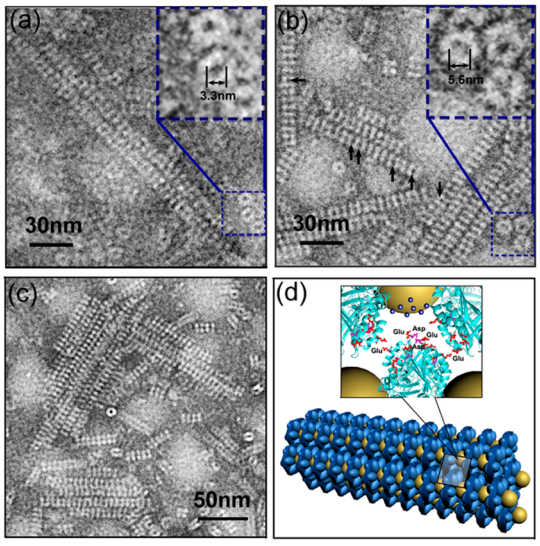

Figure 4. TEM analysis of SP1-QD assembly. (a,b) TEM images of the assembled nanostructures of SP1 with QD1 and QD2, respectively. Insets are the images of a single QD1 (a) and QD2 (b) attached to a single SP1 nanoring. The sizes of the centers of SP1 (3.3 and 5.6 nm) correspond to the sizes of QD1 and QD2 in aqueous solution. (c) TEM image of the self-assembly architectures of SP1-QD2 at high concentration. (d) Scheme representing the method of organizing arrays composed of SP1-QD2 chains. (Bottom) Bundles of nanowires of SP1-QD2 assembly. (Top) Scheme of the mechanism for the assembly of nanowire-based bundles. Glu (in red) and Asp (in purple) carry negative charges.

3D bundles of nanowires of SP1-QD2 assembly at high concentration. It is in good agreement with the AFM observation. The reasons for the formation of bundles may be as follows: first, the distance between two stacked SP1 nanorings in the SP1-QD2 assembly is 5.24 nm, calculated by the SP1 structural model using visualization software Pymol. Since the width of the SP1 nanoring is 4−5 nm, two SP1-QD2 nanowires can array staggered as gears (Figure 4d). In addition, the electrostatic interaction between the positively charged QD2 and negative charges (Glu and Asp in Figure 4d) around the outer surface of the SP1 nanoring is the actuating force. The spacial complement and electrostatic force drive the formation of the nanowire-based bundles. However, the electrostatic repulsion of the same charges around the surface of the SP1 makes the gears not insert deeply. As we know, Coulomb force is highly sensitive to the distance r which is defined by[41]

$$F(r) = \frac{Q_1 Q_2}{4\pi\varepsilon_0 \varepsilon r^2}$$

Due to the electrostatic repulsive interaction, the distance between QD2 and the outer surface of the SP1 is far, where the Coulomb force would be weak so that not all the nanowires of SP1-QD2 aggregate as bundles (Figure 4c). Generally, the AFM and TEM images indicate that the assembly of SP1-QDs is highly sensitive to the size of QDs: the straight lines, bundles of nanowires, and then to a network formed by SP1-QD3 (Figure 2g), allowing us to control the morphology of the assembly by changing the sizes of QDs.

The self-assembly behaviors of the SP1 and QDs were also studied by dynamic light scattering (DLS). Figure 5 shows typical number-averaged DLS curves. The sizes of the QDs are 3.3, 5.8, and 11.5 nm, and they are well-dispersed in aqueous solution (see the inset on the left of Figure 5). The average assembly sizes are 264, 216, and 375 nm. When the concentrations of both SP1 and QDs were increased 10-fold, visible precipitate was observed when left standing for 30 min (the inset on the right of Figure 5). The formation process of the SP1-QD assembly was monitored with

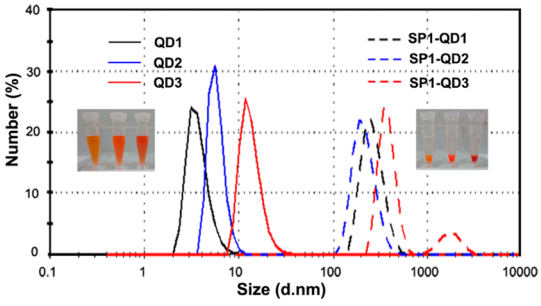

Figure 5. DLS analysis of free QDs (1 mM) and assembly of SP1 (25 mg/L) with QD1 (0.5 μM), QD2 (1.25 μM), and QD3 (2.5 μM). Insets are the pictures of QDs in aqueous solution before and after assembling with SP1.

DLS by titrating small volumes of a concentrated QD solution into a solution of the SP1 nanoring (25 mg/L). Concentration-dependent DLS curves are shown in Figure S3. The native SP1 has a diameter of 11 nm, which corresponds well to the measured hydrodynamic diameter of SP1 (10.5 nm). Following the titration of QDs, the peak corresponding to the free SP1 completely disappears and different assembly peaks are detected subsequently, which reveal the formation of SP1-QD assemblies.

In order to demonstrate the effect of ionic strengths in electrostatic self-assembly, SP1-QD1 assembly was constructed at low (10 mM), middle (50 mM), and high (250 mM) NaCl concentrations. An increase in the ionic strength of the solution reduces the electrostatic attraction between the SP1 and QD1 (Figure S4). The screening is characterized by the Debye length, κ^{-1}, which can be defined as the distance over which the Coulombic interactions are canceled by the screening effect of the counterions.[24] At 250 mM NaCl concentration, the κ^{-1} is ≈2 nm, which is not small enough to disperse all the assembly. In contrast, the κ^{-1} is ≈11 nm at 10 mM NaCl, which will not affect the electrostatic self-assembly at all.

In the natural photosynthetic centers of bacteria and plants, antenna chromophores are invariably used to absorb solar light and transfer the excitation energy to the reaction center by highly efficient singlet−singlet energy transfer.[42−47] Spatial organization of individual chromophores is crucial to such efficiency: chromophores need to be separated enough to achieve a minimum self-quenching without sacrificing the dipole−dipole coupling-mediated energy transfer. Chromophore proximity induced self-quenching and/or excimer formation is a main obstacle in light-harvesting systems if multiple donors are involved. An orderly arrangement of the QDs, which is capable of successive energy transfer to adjacent QDs, was demonstrated in this study. Therefore, these assemblies are considered an ideal scaffold for a light-harvesting antenna.

The fluorescence intensity of QDs before and after assembling with SP1 proteins was measured and is shown in Figure 6a. An appreciable increase in the luminescence of QDs was observed for all of the assemblies. The luminescence without quenching may probably be ascribed to the suitable distance between the QDs. These semiconductor particles are far enough to prevent energy loss through contact

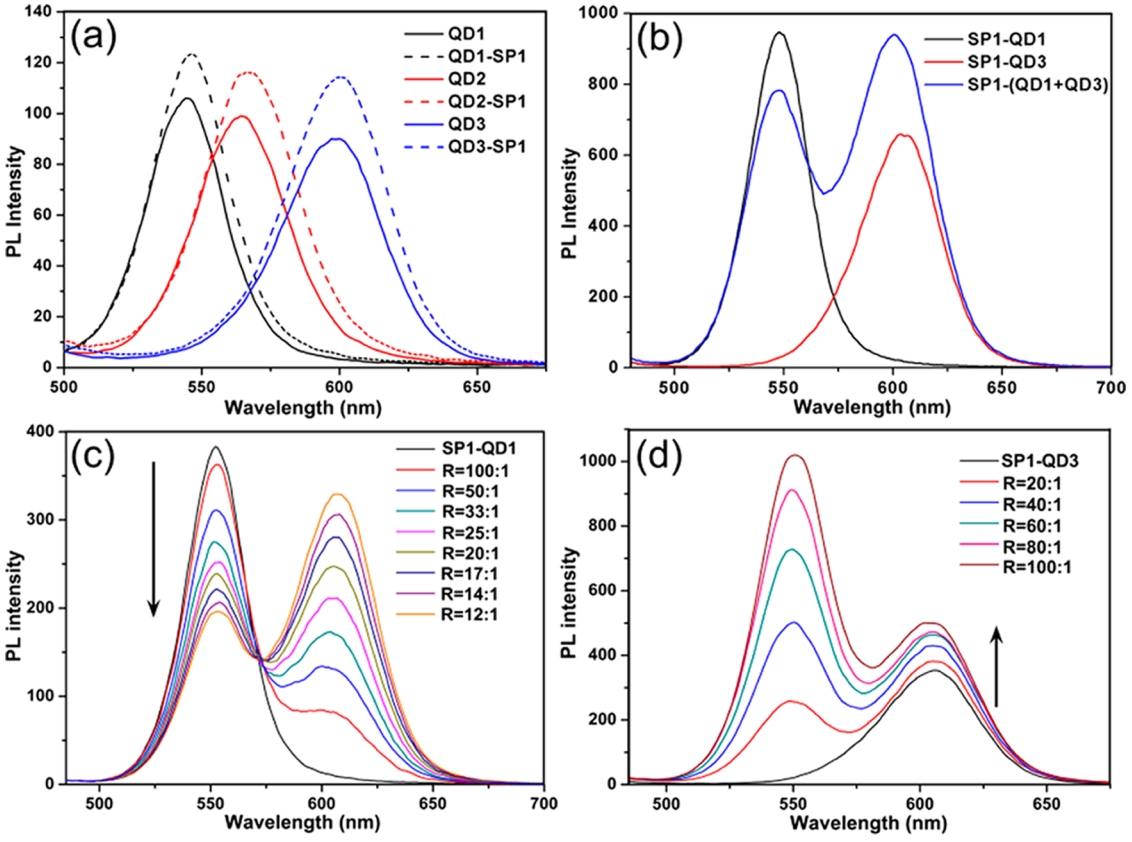

Figure 6. Fluorescence properties of the self-assembled nanowires constructed by SP1 and QDs. (a) Emission spectra of three kinds of CdTe QDs in solution (solid lines) and self-assembled nanowires with SP1 nanorings (dotted lines). (b) PL spectra of donor QD1 with SP1 (black line) and acceptor QD3 with SP1 (red line) in aqueous solutions and of their mixture solution (blue line). (c) FRET-PL spectra of the co-assembly (SP1-QD1-QD3) with different ratios of QD1/QD3. [SP1] = 25 mg/L, [QD1] = 50 μM, *R* is the number ratio of QD1 and QD3. (d) Fluorescence spectra of the co-assembled nanostructures while maintaining the concentration of SP1 (25 mg/L) and QD3 (0.5 mM) (λ_{ex} = 462 nm).

quenching. Such an increase in luminescence intensity has also been observed in previous reports dealing with the conjugation of various proteins to QDs,[48−53] wherein they attribute this phenomenon to surface passivation of the QDs and reduction of electric field effects. In addition, the absorbance spectra as shown in Figure S5 support the fluorescence data. Notably, there is a 5 nm red shift of the emission spectrum of the assemblies from 542 to 547, 562 to 567, and 600 to 605 nm, compared to that of CdTe QDs in solution. The red shift can be attributed to strong electronic coupling interaction between neighboring QDs attached to SP1. A similar observation has been reported previously by Muralidharan, who bound CdTe QDs to the bacterial flagellin fusion protein.[54]

In order to estimate the Förster radius of QDs displayed within the SP1 nanoring, the relative fluorescence QY of SP1-QDs was determined by the method reported by Williams *et al.* (Figure S6).[55] The spectral overlap integral was then calculated using the following equation:[56]

$$J(\lambda) = \int_0^\infty F_D(\lambda)\varepsilon_A(\lambda)\lambda^4 d\lambda$$

where λ is the wavelength in nanometers, ε_A ($M^{-1}\,cm^{-1}$) is the molar extinction coefficient of the acceptor at that wavelength, and F_D is the donor emission spectrum normalized on the wavelength scale

$$1 = \int_0^\infty F_D(\lambda)d\lambda$$

The overlap integral was found to be 5.06×10^{13}, 4.58×10^{13}, and $3.59 \times 10^{13}\ M^{-1}\,cm^{-1}\,nm^4$ in the case of transfer between QD1, QD2, and QD3, respectively (Table 1).

Assuming a value of 2/3 for the orientation value κ^2, an aqueous refractive index of $\eta = 1.33$, and leaving the overlap integral J in the units described above, the Förster radius (R_0), defined as the theoretical donor−acceptor distance at 50% energy transfer efficiency, was calculated using the following equation:[57]

$$R_0 = 0.211(\kappa^2 n^{-4} Q_D J(\lambda))^{1/6}\,(\text{in Å})$$

where Q_D is the QY of the donor assembled with SP1 protein. The Förster radius was thus estimated to be 2.34, 2.32, and 2.09 nm for transfer between the same QDs.

TABLE 1. Donor−Donor and Donor−Acceptor Pair Results

donor−donor/ acceptor pair	Φ^a(donor)	J (10^{13} M^{-1} cm^{-1} nm^4)	R_0 (nm)	r (nm)	E (%)
QD1−QD1	0.170	5.06	2.34	1.0	99
QD2−QD2	0.176	4.58	2.32	1.5	92
QD3−QD3	0.123	3.59	2.09	3.2	7.5
QD1−QD3	0.170	5.16	2.35	2.1	64

[a] QY of the donor assembled with SP1 protein.

The donor−acceptor distance (r) was then calculated to be 1.0, 1.5, and 3.2 nm by the SP1 structural model using visualization software Pymol. We get the result of the efficiency of energy transfer (E) by

$$E = \frac{R_0^6}{R_0^6 + r^6}$$

which shows that the transfer efficiency is strongly dependent on distance when the D−A distance is near R_0.[57] The high efficiency of energy transfer of QD1 and QD2 (99 and 92% shown in Table 1) compared to QD3 (7.5%) indicates that the size of the QDs is important for the SP1-QD assembly to form an optimal light-harvesting antenna (Figure S7).

In order to achieve efficient energy transfer, we assembled QD1 and QD3 with SP1 nanorings, sequentially. First, QD1 and QD3 were mixed well and then added to SP1 aqueous solution. In Figure 6b, three cases are compared: black line shows the photoluminescence (PL) from the donor CdTe QD1 assembled with SP1 that emits at 547 nm, while the red line gives the PL from the acceptor CdTe QD3 with SP1 emitting at 605 nm. On the other hand, the blue line presents the PL of the donor and acceptor QD pairs with SP1 together. There is an obvious increase in the emission intensity of the acceptor QD3, whereas a clear decrease is observed in the emission intensity of the donor QD1. This observation illustrates Förster energy transfer (FRET) phenomenon between these QDs. Although QD1 and QD3 can be excited at the same time, there is a pronounced FRET effect observed in the co-assembly. Most significantly, the majority of QD1 fluorescence was quenched by a few percent of QD3 (Figure 6c). One acceptor, therefore, must have quenched multiple donors in this system. Figure 6d shows the FRET, while maintaining the concentration of QD3. In comparison, no energy transfer was observed without the SP1 protein, which can be attributed to the monodispersed nature of the QDs due to electrostatic repulsion (Figure S8). In addition, the reason to select QD1−QD3 as the donor−acceptor pair rather than QD1−QD2 and QD2−QD3 is that there is less overlap between the emission peaks of QD1 and QD3 (Figure 6a).

AFM image of the co-assembly of SP1, QD1, and QD3 is shown in Figure 7a, and various nanostructures can be observed. We chose two nanowires (marked by dotted squares) and measured the height along the length of the wires. There is a 2 nm difference along the nanowires, where the lower place (∼9 nm) presents the height of the "standing" SP1 nanoring and the higher point must be QD3, which is ∼11 nm as described above. The height difference demonstrates that the QD3 connected at the head of the nanowires or in the middle linked the two nanowires according to the scheme shown in Figure 7b,c. The efficiency of energy transfer from QD1 to QD3 was calculated to be 64% (Table 1). Combined with the previous results, it is

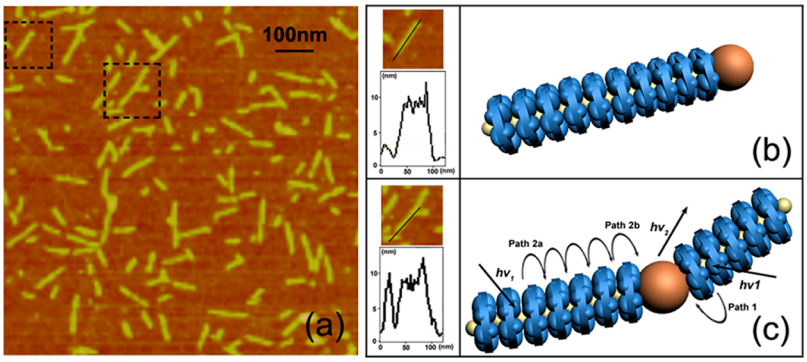

Figure 7. AFM image and data analysis of SP1-QD1-QD3 co-assembly. (a) AFM image of the SP1-QD1-QD3 assembly, where the number proportion of QD1 and QD3 is 50:1. Two nanowires marked by dotted squares were close up to measure the height along the black lines. (b,c) Two different schemes of SP1-QD1-QD3 assemblies. For systems with large numbers of donors, energy can be transferred to acceptor QD3 through direct FRET (path 1) or *via* multiple donor-to-donor transfers (paths 2a and 2b).

possible that direct energy transfer can occur from donor QD1 to acceptor QD3 (Figure 7c, path 1). Energy transfer can also occur through multiple degenerate donor-to-donor events (Figure 7c, paths 2a and 2b), which corresponds to the antenna effect and constructs a complete set of a light-harvesting system.

CONCLUSION

We demonstrate the capability of aqueous CdTe QDs to induce the self-assembly of SP1 nanorings into various nanostructures through multielectrostatic interactions. Single nanowires, nanowire-based bundles, and irregular networks are produced with various sizes of QDs (3.3, 5.8, and 11.5 nm). At the same time, the high-ordered assemblies separate QDs enough to prevent the fluorescent self-quenching phenomenon and realize a light-harvesting antenna by taking advantage of extremely efficient energy transfer among the same species of QDs. The efficiency of energy transfer between the same QDs is 99% of QD1 and 92% of QD2. Furthermore, when QD1 and QD3 are assembled together with the SP1 nanoring, obvious FRET effect was observed. The co-assembly of a protein nanoring with QD1−QD3 indicates that energy can be initially transferred among multiple QD1 donors and then to the reaction center of the QD3 acceptor by electron transfer, demonstrating the construction of a highly efficient light-harvesting system to serve as a potential platform for optical, photovoltaic, or photocatalytic devices. We expect that this strategy may be a versatile one to construct high-ordered functional protein nanomaterials in the future.

EXPERIMENTAL SECTION

Materials. Plasmid pET29a containing the SP1 protein gene was provided by Professor Oded Shoseyov (The Hebrew University of Jerusalem, Israel). Phenylmethanesulfonyl fluoride (PMSF) and isopropyl β-D-1-thiogalactopyranoside (IPTG) were purchased from Sigma (Germany). 2-Mercaptoethylamine (MA, 98%) was obtained from Acros. Sodium borohydride ($NaBH_4$, 99%) and $CdCl_2$ (99%) were commercial products. DEAE Sepharose Fast Flow was obtained from GE Healthcare, and Sephadex G75 was purchased from Amersham Pharmacia Biotech (Uppsala, Sweden). All water used was from a Millipore water purification system with a minimum resistivity of 18.0 MΩ·cm.

Overexpression and Purification of SP1 Nanoring. The SP1 domain was transformed into *Escherichia coli* BL21 (DE3), which grew to 1 L LB culture containing 50 mg/mL kanamycin with shaking at 37 °C. The protein expression was induced by adding 1 mM IPTG when OD_{600} reached 0.8. The cells were harvested 4 h after induction, and then the protein was extracted by sonication in 20 mM Tris-HCl buffer, pH 8.0, including 1 mM PMSF and 50 mM NaCl. For purification, the protein was first heated at 85 °C for 30 min and centrifuged at 15 000 rpm for 30 min. The supernatant was loaded into a 20 mL DEAE ion-exchange column running in 20 mM Tris-HCl buffer, pH 6.3, with a salt gradient from 50 to 500 mM NaCl. The target protein was eluted at 500 mM NaCl. The sample was then dialyzed by 8 kDa cutoff dialysis membrane to Milli-Q water, and further purification used Sephadex G75 with 20 mM PBS buffer, pH 7.4, including 50 mM NaCl. The purified SP1 protein was then stored at −20 °C for the experiments.

Preparation of CdTe QDs with Different Sizes. Initially, aqueous precursors of CdTe QDs were obtained by injecting a freshly prepared solution of NaHTe into 12.5 mM N_2-saturated $CdCl_2$ solutions in the presence of MA at a pH range of 5.5−6.0. The molar ratio of Cd^{2+}/MA/HTe^- was set as 1:2.4:0.2. The resultant precursor solutions were refluxed at 100 °C to maintain the growth of QDs. Their sizes increased with the reflux duration. QD1 was obtained after 40 min, QD2 after 60 min, and QD3 4 h later. After preparation, the QD solution was centrifuged at a speed of 8000 rpm with the addition of isopropyl alcohol to remove superfluous salts and MA. The precipitated QDs were then redissolved in deionized water.

Assembly of SP1-QD Nanowires. A 500 μL solution containing 50 mg/L SP1 was mixed with 500 μL of different-sized QDs in aqueous solutions at pH 6.0. The concentrations of the QDs were 1, 2.5, and 10 μM. The concentration of QDs in aqueous solution was determined analytically from the total amount of Cd. The mixed solutions were stirred vigorously for 10 min and then left to stand for 30 min.

Atomic Force Microscopy. AFM measurements were performed on a NanoScope Multimode AFM (Veeco, USA) using the tapping mode AFM with a SiN_4 tip with a radius of ~10−20 nm. Samples were prepared by immersing a freshly prepared hydroxylated silicon wafer in the SP1 (25 mg/L) and QDs (1 μM of QD1, 2.5 μM of QD2, and 10 μM of QD3) solution for a few seconds followed by drying in air.

Transmission Electron Microscopy. TEM micrographs were recorded on a JEM-2100F instrument with an accelerating voltage of 120 kV. Samples were prepared on Formvar carbon-coated copper grids by placing a 4 μL drop of a solution containing a mixture of SP1 and QDs on the grid. The sample drop was left standing for 10 min, after which time the excess buffer was blotted away with filter paper. Samples were negatively stained by applying 4 μL of stain (4% sodium phosphotungstate in Milli-Q water) onto the grid and removing the excess stain with filter paper after 40 s. The samples were dried under air flow overnight before imaging.

Dynamic Light Scattering. DLS experiments were carried out with Malvern Instrument Zetasizer Nano ZS equipped with a He–Ne laser (633 nm, 4 mW) and an Avalanche photodiode detector at an angle of 90°. Results are the average of at least five measurements. All SP1 and QDs samples were prepared in deionized water. One milliliter of SP1 solution (25 mg/L) was titrated with an aqueous QD solution (10 μM of QD1, 25 μM of QD2, and 100 μM of QD3) from 10 to 100 μL. After each titrant addition, the samples were thoroughly mixed and allowed to equilibrate for 2 min.

Light-Harvesting Probe Preparation. First, various ratios of QD1 and QD3 were well-mixed in 500 μL aqueous solution, then 500 μL of 50 mg/L SP1 was added into the solution. The solution mixture was stirred vigorously for 10 min and then left standing for 30 min at room temperature. For comparison, samples of SP1 separately assembled with QD1 and QD3 were measured at the same time. Fluorescence spectra were acquired on a Shimadzu RF-5301 PC spectrofluorimeter where the excitation wavelength was 462 nm.

Conflict of Interest: The authors declare no competing financial interest.

Acknowledgment. Special thanks go to O. Shoseyov from Smith Institute of Plant Sciences and Genetics in Agriculture, The Hebrew University of Jerusalem, for providing SP1 domain. We acknowledge financial support from the National Natural Science Foundation of China (21234004, 91027023, 21221063, and 21004028) and the 111 Project (B06009).

Supporting Information Available: SDS-PAGE and TEM image of SP1 protein; TEM images of the assembly of SP1-QD1 and SP1-QD2 at high concentration; DLS curves of SP1 solution injecting QDs gradually; DLS results for the influence of different concentrations of NaCl to the SP1-QD1 assembly; absorbance spectra of QDs and SP1-QD assemblies; fluorescence quantum yield calculations; control experiment of the FRET at different ratios of QD1/QD3. This material is available free of charge *via* the Internet at http://pubs.acs.org.

REFERENCES AND NOTES

1. Niemeyer, C. M. Functional Devices from DNA and Proteins. *Nano Today* **2007**, *2*, 42–52.
2. Reuel, N. F.; Grassbaugh, B.; Kruss, S.; Mundy, J. Z.; Opel, C.; Egodage, K.; Wahl, R.; Helk, B.; Zhang, J. Q.; Strano, M. S.; *et al.* Emergent Properties of Nanosensor Arrays: Applications for Minitoring IgG Affinity Distributions, Weakly Affined Hypermannosylation, and Colony Selection for Biomanufacturing. *ACS Nano* **2013**, *7*, 7472–7482.
3. Wilner, O. I.; Weizmann, Y.; Gill, R.; Lioubashevski, O.; Freeman, R.; Willner, I. Enzyme Cascades Activated on Topologically Programmed DNA Scaffolds. *Nat. Nanotechnol.* **2009**, *4*, 249–254.
4. Guo, P. The Emerging Field of RNA Nanotechnology. *Nat. Nanotechnol.* **2010**, *5*, 833–842.
5. Lee, J. H.; Wong, N. Y.; Tan, L. H.; Wang, Z.; Lu, Y. Controlled Alignment of Multiple Proteins and Nanoparticles with Nanometer Resolution *via* Backbone-Modified Phosphorothioate DNA and Bifunctional Linkers. *J. Am. Chem. Soc.* **2010**, *132*, 8906–8908.
6. Suci, P. A.; Kang, S.; Young, M.; Douglas, T. A Streptavidin-Protein Cage Janus Particle for Polarized Targeting and Modular Functionalization. *J. Am. Chem. Soc.* **2009**, *131*, 9164–9165.
7. Li, Q.; So, C. R.; Fegan, A.; Cody, V.; Sarikaya, M.; Vallera, D. A.; Wagner, C. R. Chemically Self-Assembled Antibody Nanorings (CSANs): Design and Characterization of an Anti-CD3 IgM Biomimetic. *J. Am. Chem. Soc.* **2010**, *132*, 17247–17257.
8. Burazerovic, S.; Gradinaru, J.; Pierron, J.; Ward, T. R. Hierarchical Self-Assembly of One-Dimensional Streptavidin Bundles as a Collagen Mimetic for the Biomineralization of Calcite. *Angew. Chem., Int. Ed.* **2007**, *46*, 5510–5514.
9. Biswas, S.; Kinbara, K.; Niwa, T.; Taguchi, H.; Ishii, N.; Watanabe, S.; Miyata, K.; Kataoka, K.; Aida, T. Biomolecular Robotics for Chemomechanically Driven Guest Delivery Fuelled by Intracellular ATP. *Nat. Chem.* **2013**, *5*, 613–620.
10. Ballister, E. R.; Lai, A. H.; Zuckermann, R. N.; Cheng, Y. F.; Mougous, J. D. *In Vitro* Self-Assembly of Tailorable Nanotubes from a Simple Protein Building Block. *Proc. Natl. Acad. Sci. U.S.A.* **2008**, *105*, 3733–3738.
11. Kitagishi, H.; Kakikura, Y.; Yamaguchi, H.; Oohora, K.; Harada, A.; Hayashi, T. Self-Assembly of One- and Two-Dimensional Hemoprotein Systems by Polymerization through Heme–Heme Pocket Interactions. *Angew. Chem., Int. Ed.* **2009**, *48*, 1271–1274.
12. Padilla, J. E.; Colovos, C.; Yeates, T. O. Nanohedra: Using Symmetry To Design Self Assembling Protein Cages, Layers, Crystals, and Filaments. *Proc. Natl. Acad. Sci. U.S.A.* **2001**, *98*, 2217–2221.
13. Hou, C. X.; Li, J. X.; Zhao, L. L.; Zhang, W.; Luo, Q.; Dong, Z. Y.; Xu, J. Y.; Liu, J. Q. Construction of Protein Nanowires through Cucurbit[8]uril-Based Highly Specific Host–Guest Interactions: An Approach to the Assembly of Functional Proteins. *Angew. Chem., Int. Ed.* **2013**, *52*, 5590–5593.
14. Bai, Y. S.; Luo, Q.; Zhang, W.; Miao, L.; Xu, J. Y.; Li, H. B.; Liu, J. Q. Highly Ordered Protein Nanorings Designed by Accurate Control of Glutathione S-Transferase Self-Assembly. *J. Am. Chem. Soc.* **2013**, *135*, 10966–10969.
15. Zhang, W.; Luo, Q.; Miao, L.; Hou, C. X.; Bai, Y. S.; Dong, Z. Y.; Xu, J. Y.; Liu, J. Q. Self-Assembly of Glutathione S-Transferase into Nanowires. *Nanoscale* **2012**, *4*, 5847–5851.
16. Han, S. P.; Maune, H. T.; Barish, R. D.; Bockrath, M.; Goddard, W. A. DNA-Linker-Induced Surface Assembly of Ultra Dense Parallel Single Walled Carbon Nanotube Arrays. *Nano Lett.* **2012**, *12*, 1129–1135.
17. Ghosh, P. S.; Kim, C. K.; Han, G.; Forbes, N. S.; Rotello, V. M. Efficient Gene Delivery Vectors by Tuning the Surface Charge Density of Amino Acid-Functionalized Gold Nanoparticles. *ACS Nano* **2008**, *2*, 2213–2218.
18. Doni, G.; Kostiainen, M. A.; Danani, A.; Pavan, G. M. Generation-Dependent Molecular Recognition Controls Self-Assembly in Supramolecular Dendron-Virus Complexes. *Nano Lett.* **2011**, *11*, 723–728.
19. De, M.; Rana, S.; Akpinar, H.; Miranda, O. R.; Arvizo, R. R.; Bunz, U. H. F.; Rotello, V. M. Sensing of Proteins in Human Serum Using Conjugates of Nanoparticles and Green Fluorescent Protein. *Nat. Chem.* **2009**, *1*, 461–465.
20. Pack, D. W.; Hoffman, A. S.; Pun, S.; Stayton, P. S. Design and Development of Polymers for Gene Delivery. *Nat. Rev. Drug Discovery* **2005**, *4*, 581–593.
21. Mammen, M.; Choi, S. K.; Whitesides, G. M. Polyvalent Interactions in Biological Systems: Implications for Design and Use of Multivalent Ligands and Inhibitors. *Angew. Chem., Int. Ed.* **1998**, *37*, 2754–2794.
22. Srivastava, S.; Santos, A.; Critchley, K.; Kim, K.-S.; Podsiadlo, P.; Sun, K.; Lee, J.; Xu, C.; Lilly, G. D.; Glotzer, S. C.; *et al.* Light-Controlled Self-Assembly of Semiconductor Nanoparticles into Twisted Ribbons. *Science* **2010**, *327*, 1355–1359.
23. Kostiainen, M. A.; Kasyutich, O.; Cornelissen, J. J. L. M.; Nolte, R. J. M. Self-Assembly and Optically Triggered Disassembly of Hierarchical Dendron–Virus Complexes. *Nat. Chem.* **2010**, *2*, 394–399.
24. Kostiainen, M. A.; Pietsch, C.; Hoogenboom, R.; Nolte, R. J. M.; Cornelissen, J. J. L. M. Temperature-Switchable Assembly of Supramolecular Virus–Polymer Complexes. *Adv. Funct. Mater.* **2011**, *21*, 2012–2019.
25. Kostiainen, M. A.; Hiekkataipale, P.; Torre, J. A.; Nolte, R. J. M.; Cornelissen, J. J. L. M. Electrostatic Self-Assembly

of Virus–Polymer Complexes. *J. Mater. Chem.* **2011**, *21*, 2112–2117.
26. Kostiainen, M. A.; Ceci, P.; Fornara, M.; Hiekkataipale, P.; Kasyutich, O.; Nolte, R. J. M.; Cornelissen, J. J. L. M.; Desautels, R. D.; Lierop, J. Hierarchical Self-Assembly and Optical Disassembly for Controlled Switching of Magnetoferritin Nanoparticle Magnetism. *ACS Nano* **2011**, *5*, 6394–6402.
27. Dgany, O.; Gonzalez, A.; Sofer, O.; Wang, W.; Zolotnitsky, G.; Wolf, A.; Shoham, Y.; Altman, A.; Wolf, S. G.; Shoseyov, O.; *et al.* The Structural Basis of the Thermostability of SP1, a Novel Plant (Populustremula) Boiling Stable Protein. *J. Biol. Chem.* **2004**, *279*, 51516–51523.
28. Heyman, A.; Medalsy, I.; Or, O. B.; Dgany, O.; Gottlieb, M.; Porath, D.; Shoseyov, O. Protein Scaffold Engineering towards Tunable Surface Attachment. *Angew. Chem., Int. Ed.* **2009**, *48*, 1–6.
29. Medalsy, I.; Dgany, O.; Sowwan, M.; Cohen, H.; Yukashevska, A.; Wolf, S. G.; Wolf, A.; Koster, A.; Shoseyov, O.; Porath, D.; *et al.* SP1 Protein-Based Nanostructures and Arrays. *Nano Lett.* **2008**, *8*, 473–477.
30. Khoutorsky, A.; Heyman, A.; Shoseyov, O.; Spira, M. E. Formation of Hydrophilic Nanochannels in the Membrane of Living Cells by the Ringlike Stable Protein-SP1. *Nano Lett.* **2011**, *11*, 2901–2904.
31. Medintz, I. L.; Uyeda, H. T.; Goldman, E. R.; Mattoussi, H. Quantum Dot Bioconjugates for Imaging, Labelling and Sensing. *Nat. Mater.* **2005**, *4*, 435–446.
32. Achermann, M.; Petruska, M. A.; Kos, S.; Smith, D. L.; Koleske, D. D.; Klimov, V. I. Energy-Transfer Pumping of Semiconductor Nanocrystals Using an Epitaxial Quantum Well. *Nature* **2004**, *429*, 642–646.
33. Achermann, M.; Petruska, M. A.; Koleske, D. D.; Crawford, M. H.; Klimov, V. I. Nanocrystal-Based Light-Emitting Diodes Utilizing High-Efficiency Nonradiative Energy Transfer for Color Conversion. *Nano Lett.* **2006**, *6*, 1396–1400.
34. Nam, K. T.; Kim, D. W.; Yoo, P. J.; Chiang, C. Y.; Meethong, N.; Hammond, P. T.; Chiang, Y. M.; Belcher, A. M. Virus-Enabled Synthesis and Assembly of Nanowires for Lithium Ion Battery Electrodes. *Science* **2006**, *312*, 885–888.
35. Dennis, A. M.; Rhee, W. J.; Sotto, D.; Dublin, S. N.; Bao, G. Quantum Dot Fluorescent Protein FRET Probes for Sensing Intracellular pH. *ACS Nano* **2012**, *6*, 2917–2924.
36. Dennis, A. M.; Bao, G. Quantum Dot-Fluorescent Protein Pairs as Novel Fluorescence Resonance Energy Transfer Probes. *Nano Lett.* **2008**, *8*, 1439–1445.
37. Jiang, G. X.; Susha, A. S.; Lutich, A. A.; Stefani, F. D.; Feldmann, J.; Rogach, A. L. Cascaded FRET in Conjugated Polymer/Quantum Dot/Dye-Labeled DNA Complexes for DNA Hybridization Detection. *ACS Nano* **2009**, *3*, 4127–4131.
38. Curto, A. G.; Volpe, G.; Taminiau, T. H.; Kreuzer, M. P.; Quidant, R.; Hulst, N. F. V. Unidirectional Emission of a Quantum Dot Coupled to a Nanoantenna. *Science* **2010**, *329*, 930–932.
39. Zou, Q. L.; Zhang, L.; Yan, X. H.; Wang, A. H.; Ma, G. H.; Li, J. B.; Möhwald, H.; Mann, S. Multifunctional Porous Microspheres Based on Peptide–Porphyrin Hierarchical Coassembly. *Angew. Chem., Int. Ed.* **2014**, *53*, 2366–2370.
40. Huang, X.; Li, M.; Green, D. C.; Williams, D. S.; Patil, A. J.; Mann, S. Interfacial Assembly of Protein–Polymer Nanoconjugates into Stimulus-Responsive Biomimetic Protocells. *Nat. Commun.* **2013**, *4*, 2239–2247.
41. Israelachvili, J. N. *Intermolecular and Surface Forces*, 3rd ed.; Academic Press: London, 2011; p 55.
42. McDermott, G.; Prince, S. M.; Freer, A. A.; Hawthornthwaite-Lawless, A. M.; Papiz, M. Z.; Cogdell, R. J.; Isaacs, N. W. Crystal Structure of an Integral Membrane Light-Harvesting Complex from Photosynthetic Bacteria. *Nature* **1995**, *374*, 517–521.
43. Pullerits, T.; Sundstrom, V. Photosynthetic Light-Harvesting Pigment–Protein Complexes: Toward Understanding How and Why. *Acc. Chem. Res.* **1996**, *29*, 381–389.
44. Hu, X. C.; Damjanovic, A.; Ritz, T.; Schulten, K. Architecture and Mechanism of the Light-Harvesting Apparatus of Purple Bacteria. *Proc. Natl. Acad. Sci. U.S.A.* **1998**, *95*, 5935–5941.
45. van Oijen, A. M.; Ketelaars, M.; Kohler, J.; Aartsma, T. J.; Schmidt, J. Unraveling the Electronic Structure of Individual Photosynthetic Pigment–Protein Complexes. *Science* **1999**, *285*, 400–402.
46. Polvka, T.; Frank, H. A. Molecular Factors Controlling Photosynthetic Light Harvesting by Carotenoids. *Acc. Chem. Res.* **2010**, *43*, 1125–1134.
47. Scholes, G. D.; Fleming, G. R.; Olaya-Castro, A.; van Grondelle, R. Lessons from Nature about Solar Light Harvesting. *Nat. Chem.* **2011**, *3*, 763–774.
48. Goldman, E. R.; Medintz, I. L.; Hayhurst, A.; Anderson, G. P.; Mauro, J. M.; Iverson, B. L.; Georgiou, G.; Mattoussi, H. Self-Assembled Luminescent CdSe–ZnS Quantum Dot Bioconjugates Prepared Using Engineered Poly-histidine Terminated Proteins. *Anal. Chim. Acta* **2005**, *534*, 63–67.
49. Mattoussi, H.; Mauro, J. M.; Goldman, E. R.; Anderson, G. P.; Sundar, V. C.; Mikulec, F. V.; Bawendi, M. G. Self-Assembly of CdSe–ZnS Quantum Dot Bioconjugates Using an Engineered Recombinant Protein. *J. Am. Chem. Soc.* **2000**, *122*, 12142–12150.
50. Wang, L.; Wang, L. Y.; Zhu, C. Q.; Wei, X. W.; Kan, X. W. Preparation and Application of Functionalized Nanoparticles of CdS as a Fluorescence Probe. *Anal. Chim. Acta* **2002**, *468*, 35–41.
51. Wang, L. Y.; Kan, X. W.; Zhang, M. C.; Zhu, C. Q.; Wang, L. Fluorescence for the Determination of Protein with Functionalized Nano-ZnS. *Analyst* **2002**, *127*, 1531–1534.
52. Hanaki, K.; Momo, A.; Oku, T.; Komoto, A.; Maenosono, S.; Yamaguchi, Y.; Yamamoto, K. Semiconductor Quantum Dot/Albumin Complex Is a Long-Life and Highly Photostable Endosome Marker. *Biochem. Biophys. Res. Commun.* **2003**, *302*, 496–501.
53. Mamedova, N. N.; Kotov, N. A.; Rogach, A. L.; Studer, J. Albumin–CdTe Nanoparticle Bioconjugates: Preparation, Structure, and Interunit Energy Transfer with Antenna Effect. *Nano Lett.* **2001**, *1*, 281–286.
54. Kumara, M. T.; Tripp, B. C.; Muralidharan, S. Exciton Energy Transfer in Self-Assembled Quantum Dots on Bioengineered Bacterial Flagella Nanotubes. *J. Phys. Chem. C* **2007**, *111*, 5276–5280.
55. Mottram, L.; Boonyarattanakalin, S.; Kovel, R. E.; Peterson, B. R. The Pennsylvania Green Fluorophore: A Hybrid of Oregon Green and Tokyo Green for the Construction of Hydrophobic and pH-Insensitive Molecular Probes. *Org. Lett.* **2006**, *8*, 581–584.
56. Montali, A.; Harms, G. S.; Renn, A.; Weder, C.; Smith, P.; Wild, U. P. Time-Resolved Fluorescence Study on the Mechanism of Polarizing Energy Transfer in Uniaxially Oriented Polymer Blends. *Phys. Chem. Chem. Phys.* **1999**, *1*, 5697–5702.
57. Lakowicz, J. R. *Principles of Fluorescence Spectroscopy*; Plenum Press: New York, 1983; pp 446–447.